# Prediction of heat transfer in a turbine cascade with high levels of free-stream turbulence

**By G. Medic†, J. Joo†, S. K. Lele AND O. P. Sharma†**

Large-eddy simulation has been applied to predict flow and heat transfer in a turbine cascade with high levels of free-stream turbulence. This configuration has been derived from UTRC experiments of Blair *et al.* (1989*a*,*b*). In these experiments free-stream turbulence had a dramatic impact on the location of transition on the suction side. Simulations presented here show that it is critical to match the experimentally observed characteristics of turbulent flow at the measurement station just upstream of the leading edge of the vane. Similarly, the importance of maintaining sufficient grid resolution both upstream of the leading edge and along the vane surface has also been illustrated.

## 1. Introduction

Heat transfer in a high-pressure turbine configuration (from the experiment by Blair *et al.* (1989*a*,*b*), conducted at UTRC) has been analyzed by means of large-eddy simulation. Blair's low-speed large-scale rotating rig (LSRR) consists of a first stator, a rotor and an exit stator. It was built to conduct basic experiments to study the development of boundary layers and secondary flows in advanced low-aspect ratio turbines. The large scale allowed acquisition of high-resolution steady and unsteady flow and heat transfer data in a rotating rig environment. Flow and heat transfer were assessed in detail for two configurations — with and without the presence of the turbulence generating grid. A particular challenge here is that the turbulence grid generates fairly high levels of inlet turbulence with turbulence intensity (TU) of about 10% just upstream of the leading edge of the first stator; this moves the transition location upstream in a dramatic fashion. In addition, the flow has been analyzed for a range of Reynolds numbers by changing the inlet velocity. Finally, as far as the rotor blade is concerned, the flow and heat transfer were also analyzed experimentally for a range of incidence angles assessing the pressure side heat transfer increase at negative incidence angles (which was achieved by modifying the rotational speed of the rotor wheel).

The scope of the simulations presented here is similar to, and draws upon, what has been learned from recent LES analyses of heat transfer for turbine vane configurations from VKI (Arts *et al.* 1990) by Bhaskaran & Lele (2011) and Collado Morata *et al.* (2012). In the LES computations presented here, the vane geometry was also modeled with a 2D single passage cascade constructed using the mid-span section. The nominal operating conditions have Reynolds number of approximately 650,000; this sets the requirements for computational grids for wall-resolved LES. Following the guidelines set by Wu & Moin (2009, 2010), and more recently by Sayadi & Moin (2011) and Sayadi *et al.* (2011), the intent with the grids used here was to keep the streamwise, $\Delta s^+$, and spanwise, $\Delta z^+$, grid resolution below 50 and 10, respectively — the grid count for these single-passage analyses ranges from 80 to 320 millions of computational cells.

† United Technologies Research Center, East Hartford, CT

Inlet turbulence plays a critical role in the simulations for the first stator. There are extensive measurements of the state of turbulence approaching the leading edge in Blair *et al.* (1989*a*), but properly representing it in a numerical simulation is a non-trivial task. Various approaches have been devised over time for the generation of inlet turbulence with the synthesization of inlet fluctuations (Klein *et al.* 2003) and the use of auxiliary precursor simulations (Morgan *et al.* 2011) being the most widespread. In this work, the latter approach was taken. Detailed sensitivity studies illustrating changes in the transition location and heat transfer with changes to turbulence isotropy, homogeneity, TU levels, turbulence length scale, and grid resolution have been conducted.

### 1.1. *Methodology*

The flow solver used in these simulations is based on a second-order-accurate (both in space and time), explicit-in-time, numerical method for compressible flow equations, first presented in Ni (1982). The core of the current multi-block structured solver has been extensively validated for turbomachinery flows over the past 30 years.

In the LES framework, Navier-Stokes equations for the filtered velocity are solved in the entire computational domain, and unresolved turbulence scales are modeled with a subgrid scale model. Here, the WALE model of Nicoud & Ducros (1999) is employed for the subgrid scale viscosity:

$$\nu_t^{SGS} = (C_w \Delta)^2 \frac{\left(S_{ij}^d S_{ij}^d\right)^{3/2}}{\left(\bar{S}_{ij}\bar{S}_{ij}\right)^{5/2} + \left(S_{ij}^d S_{ij}^d\right)^{5/4}}, \tag{1.1}$$

where $\bar{S}_{ij}$ is the strain rate tensor for the resolved field, and $C_w = 0.5$. $S_{ij}$ is defined as

$$S_{ij}^d = \frac{1}{2}\left(\bar{g}_{ij}^2 + \bar{g}_{ji}^2\right) - \frac{1}{3}\delta_{ij}\bar{g}_{kk}^2, \tag{1.2}$$

with $\bar{g}_{ij}^2 = \frac{\partial \bar{u}_i}{\partial x_k}\frac{\partial \bar{u}_k}{\partial x_j}$ and $\delta_{ij}$ the Kronecker symbol.

For the subgrid scale heat flux, the assumption is made that the energy transfer from the resolved scales to the subgrid scales is proportional to the gradient of resolved temperature with the proportionality coefficient being the subgrid scale conductivity:

$$\kappa_t^{SGS} = \frac{\rho \nu_t^{SGS} C_p}{Pr_{SGS}}, \tag{1.3}$$

where $Pr_{SGS}$ is the subgrid scale Prandtl number which is usually chosen in the interval $[0.3, 0.9]$ — a value of 0.9 is used here.

A low-pass filtering technique introduced in Lele (1992), and implemented as in Joo (2008), can be applied periodically to suppress the high-frequency numerical instabilities when necessary. Among the group of filtering schemes introduced in Lele (1992), the fourth-order tridiagonal scheme ($\alpha = 0.475$ and $d = 0$) is used in this context. An example of such one-dimensional filtering (applied along each computational coordinate line) is defined as

$$a\hat{y}(i-1) + b\hat{y}(i) + c\hat{y}(i+1) = dy(i-2) + ey(i-1) + fy(i) + gy(i+1) + hy(i+2), \tag{1.4}$$

where $\hat{y}$ is the filtered value of a variable and $y$ is its value before filtering; the values of the coefficients $a - h$ are discussed in detail in Joo (2008).

As discussed in detail by Medic & Sharma (2012), the solver has been tested successfully for standard benchmarking tests for LES: (a) decay of homogeneous isotropic turbulence, and (b) turbulent flow in a periodic channel at $Re_\tau = u_\tau h/\nu$ of 395.

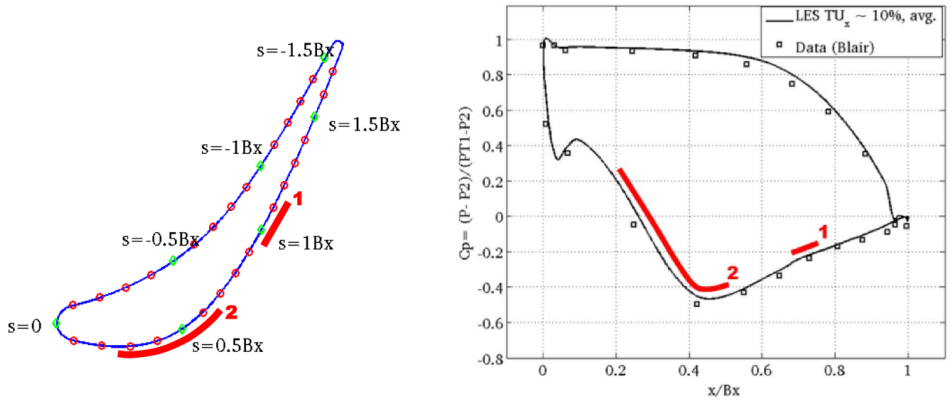


FIGURE 1. Definition of curvilinear coordinate $s$ (left) where $B_x$ is the axial chord of the airfoil, and plot of pressure coefficient $C_P = (P - P_2)/(P_{T1} - P_2)$ vs axial coordinate $x$, computed on baseline grid (right). Stripes 1 and 2 indicate where transition takes place in the experiment — without and with the presence of turbulence grid.

In addition, it has been applied to a variety of low-pressure turbine cascade configurations; see further discussion in Medic & Sharma (2012) where flow over three low-pressure turbine airfoils was analyzed for a range of Reynolds numbers (30,000 to 150,000). The baseline computational grid for those 2D linear cascade configurations consisted of 35 millions cells, and additional finer grids of 70 millions cells were used for grid-sensitivity studies. The configurations were analyzed for low free-stream turbulence intensity, as well as for 4% turbulence intensity at free-stream. In these LPT simulations, a laminar separation exists on the suction side, and, depending on the Reynolds number, the flow at the outer edge of the separation either transitions, and the separation closes before the trailing edge, or not. Detailed comparison to measurements of computed surface pressure and total pressure losses over the range of Reynolds numbers for all three airfoils showed that these LES analyses were able to capture the separation-induced transition and the overall trends in changes for loss dependence on Reynolds number from one airfoil to another. Simulations with inlet turbulence were also conducted, but its impact of delaying the laminar flow separation was not captured accurately.

### 1.2. *LSRR turbine cascade — first stator*

The geometry of the vane in the first stator, and the definition of the curvilinear coordinate $s$ along the stator vane airfoil surface, are shown in Figure 1. The portion of the airfoil over which transition occurs without (1) and with (2) the turbulence-generating grid is also illustrated. These locations are inferred from the data presented in Figure 6 – note that with the turbulence-generating grid the transition is initiated in a region of strong favorable pressure gradient. Baseline flow conditions are given in Blair *et al.* (1989*a*).

In this work, an O-H grid topology has been chosen as a starting point for the single passage domain. The baseline grid was constructed using 1600 × 192 cells in the O-block, and 1216 x 256 cells in the H-block, with 128 cells in the spanwise direction (for the spanwise extent of 0.05 Bx), resulting in a baseline grid with approximately 80 million computational cells. A finer grid in the streamwise direction has also been analyzed —

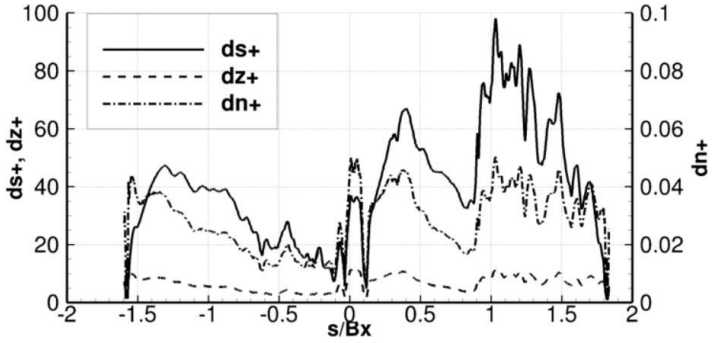


FIGURE 2. Grid resolution for baseline grid from simulations with 10% inlet turbulence.

with 2432 cells in the H-block, and 3200 cells along the airfoil surface in the O-block. In addition, a domain with a wider spanwise extent of 0.1 Bx was also analyzed (with 256 computational cells). As a result, the grids used in these analyses range from 80 to 320 millions of computational cells. Figure 2 shows the grid resolution for the baseline grid (80 million cells) along the vane surface in plus units — computed for the instantaneous solution in one of the runs with inlet turbulence. For the grid with twice the streamwise resolution, $\Delta s^+$ is twice as small, i.e., lower than 50. Note that the fine grid is consistent with the recommendations made by Sayadi & Moin (2011) for their LES analyses of natural transition.

Temporal resolution in the same simulation on the baseline grid shows that the time-step is $\Delta t^+ < 0.25$. With this time-step, it takes approximately 20,000 time-steps for a particle to travel from domain inflow to domain outflow, and about one third of that time (≈6,000 time-steps) to traverse the length of the vane. If that is defined as a passage flow-through time, the total time of a simulation is about 7 flow-through times, with time-averages computed over approximately the last three of those flow-through times. As can be deduced from results in Figures 6 and 8, more flow-through times might be needed for improved time-averaging. The computational cost of the simulation with the baseline grid is approximately 10,000 CPU hours, whereas the simulation on the finer grid with a wider spanwise extent takes about 40,000 to 45,000 CPU hours.

### 1.3. *Inlet turbulence*

As discussed, one of the objectives of this work is to assess the ability of the present solver and the WALE subgrid-scale model to predict the impact of inlet turbulence on bypass transition in the boundary layer and subsequently the heat transfer on the stator vane surface. Experimental data document the levels of streamwise fluctuations $u_{rms}/U$, as well as turbulence length scale, just upstream of the leading edge of the first stator (at $x/B_x = -0.23$), which was induced by a turbulent grid installed further upstream [Blair *et al.* (1989*a*) even show that the turbulent fluctuations of streamwise velocity follow a Von Karman spectrum]. Not much is known about the homogeneity and isotropy, although the authors show a variation of TU at various spanwise locations from 8.5 to 10.5%, and a variation of length scale from 0.125 to 0.145 $B_x$. In this work the values of 10% and 0.1 $B_x$ were adopted.

Turbulent fluctuations were generated from an auxiliary simulation of decay of homogeneous and isotropic turbulence in a box, and then superimposed to mean flow computed with LES with no inlet turbulence. The approach taken relied on storing one instantaneous snapshot of 3D turbulent fluctuations and then sweeping in one spatial direction

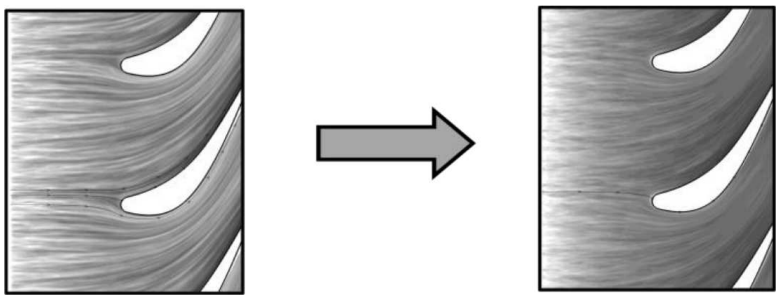

FIGURE 3. Time-averaged turbulence intensity - improvement in the homogeneity of the inlet turbulence dataset.

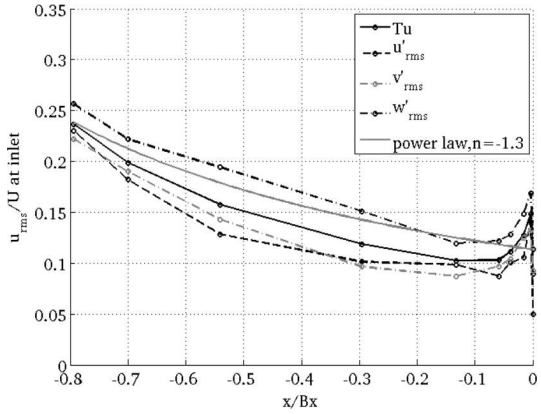


FIGURE 4. Decay of turbulence upstream of the leading edge — on baseline grid.

to produce time-dependence. An initial dataset was constructed with a box of modest size ($128^3$) — imperfections with respect to the homogeneity of inlet turbulence were observed. This was manifested by *striping* in time-averaged turbulent intensity in the stator simulation, upstream of the leading edge (Figure 3, left). Refined inlet turbulence generation process was then designed to insure improved homogeneity of turbulence intensity — a larger box was constructed using multiple auxiliary simulations, resulting in a dataset that covers a 10 times larger time period (similar to the blending of multiple realization in small boxes discussed in Xiong & Lele (2007)). Using this new inlet turbulence dataset improved the spatial homogeneity of time-averaged turbulence intensity upstream of the stator leading edge, as shown on the right of Figure 3.

Measurements of the levels of $u_{rms}/U$ fluctuations were conducted at $x/B_x = -0.23$, while the domain inlet in this configuration is at approximately -0.88. After an initial adjustment at the inlet — the actual boundary values were computed by superimposing linearly the mean flow solution and the auxiliary DHIT dataset, which in itself is then not a solution of the equations — turbulence decays by following a power law (see Figure 4). Note that a certain anisotropy develops — the resolution in the $z$ direction at the inlet is much finer than in the other two directions (i.e., $\Delta z$ is about 10 times smaller than $\Delta y$ and $\Delta x$ for the baseline grid); as a result, spanwise fluctuations are somewhat higher than the other two components.

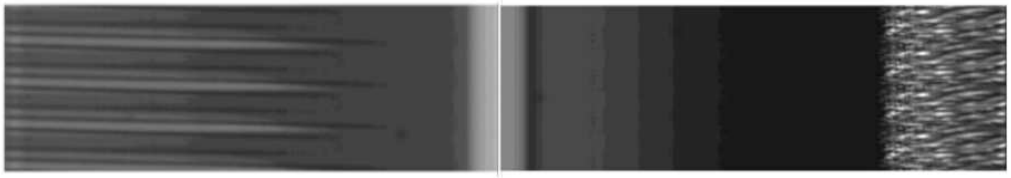

FIGURE 5. Instantaneous heat transfer coefficient along the vane surface — computed with no inlet turbulence.

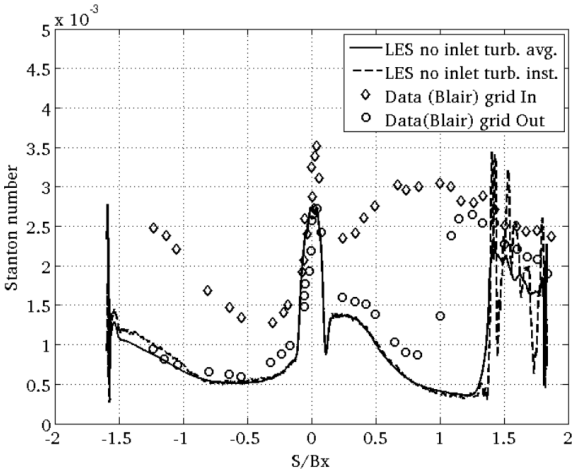


FIGURE 6. Stanton number — no inlet turbulence.

## 2. Heat transfer predictions

The initial simulation was performed with no inlet turbulence using the baseline grid, and then turbulent fluctuations were gradually added to match $u_{rms}/U$ of 10% observed at $x/B_x = -0.23$ in experiments. Because of the challenges described above, setting the inlet turbulence levels to match the data just upstream of leading edge was an iterative process. A set of simulations with different levels of $u_{rms}/U$ was generated. Finally, the spanwise domain was extended to 0.1 $B_x$, and the grid was refined in the streamwise direction (as discussed in 1.2).

### 2.1. *No inlet turbulence*

Contours of the instantaneous surface heat transfer coefficient $h = q''/(T_{wall} - T_1)$ on the suction and pressure sides are presented in Figure 5 for the *unwrapped* vane (LE is in the middle, the pressure side is on the left, and the suction side on the right, with four copies of the domain plotted in the spanwise direction). The computed time- and spanwise-averaged Stanton number $St = h/(c_p \rho U_2)$ is compared to experimental data from the case without the turbulence grid in Figure 6 (experimental values of the Stanton number for the case with the turbulence grid in are also shown for reference). The flow at the leading edge and on the pressure side remains laminar and the simulation results compare well to data at the leading edge. Interestingly, the simulations predict the increase of the Stanton number towards the back of the pressure side — which a laminar boundary layer code fails to capture. At the same time, in the plots of the instantaneous surface heat transfer coefficient there is an appearance of streaky structures on the pressure side, reminiscent of Görtler vortices.

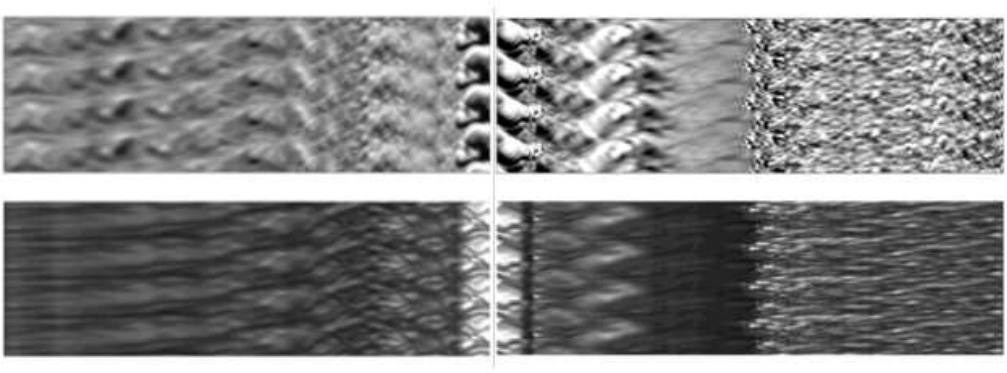

FIGURE 7. Instantaneous contours of spanwise velocity fluctuations at $\Delta y_n = 0.0018 B_x$ off the vane surface (top), and the heat transfer coefficient along the vane surface (bottom) — computed with $u_{rms}/U = 10\%$ using the baseline grid.

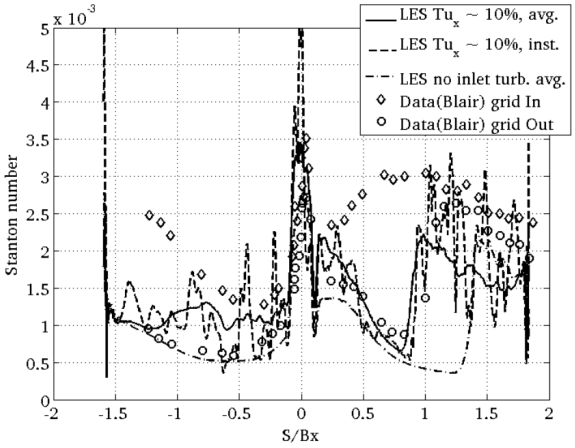


FIGURE 8. Stanton number for $u_{rms}/U = 10\%$ — baseline grid.

On the suction side, flow transitions at $s/B_x$ of approximately 1.4, whereas the data show transition closer to 1.15. Clearly, the experimental data were not taken in the complete absence of free-stream disturbances. In Blair *et al.* (1989*a*), there is some information on the state of turbulence approaching the leading edge for the case with no turbulence grid — $u_{rms}/U$ is in the range from 0.5 to 1%. There is not much information on turbulence length scale — there is some speculation about long-wave disturbances generated by the outline of the facility. Note also that after the transition, the levels of Stanton number appear somewhat low, confirming that the streamwise resolution of the baseline grid in the fully turbulent region (with peak $\Delta s^+$ of 90) is too coarse to properly resolve the turbulent boundary layer structures.

### 2.2. *Sensitivity to inlet turbulence*

Results with 10% of $u_{rms}/U$ computed using the baseline grid are presented next. Instantaneous contours of surface heat flux are shown in Figure 7; the transition location has moved upstream but not as far upstream as in the experiments. From the experimental results we see that transition ends at $s$ of about 0.65 $B_x$, whereas the simulations show fully turbulent flow at about 0.95 $B_x$. Indeed, gradually adding higher levels of

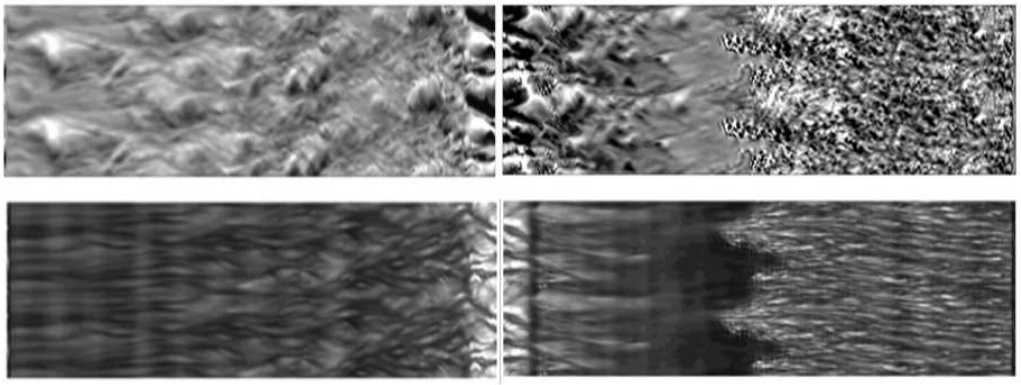

FIGURE 9. Instantaneous contours of spanwise velocity fluctuations at $\Delta y_n = 0.0018 B_x$ off the vane surface (top), and heat transfer coefficient along the vane surface (bottom) — computed with $u_{rms}/U = 10\%$, streamwise grid refinement, and larger spanwise extent.

inlet turbulence shows a gradual movement of transition location from 1.4 to 0.95 $B_x$. Instantaneous values of Stanton number for this simulation are shown in Figure 8. The underprediction of Stanton number in the fully turbulent region is now more clearly visible. Note also the drop in heat transfer towards the end of the pressure side, with the flow, seemingly relaminarizing.

The next step was to extend the domain in $Z$ to 0.1 $B_x$, and refine the grid in the streamwise direction to ensure that even in the turbulent portion of the boundary layer $\Delta s^+$ remains under 50. At the same time, this refinement improved the accuracy of turbulent fluctuations reaching the leading edge. Instantaneous contours of the surface heat transfer coefficient shown in Figure 9 confirm forward motion of the transition location, as well as more resolved structures in the region of the breakdown of instabilities occurring more upstream on the suction side. Note that in Figure 9 there are only 2 copies of the domain in $Z$.

## 3. Concluding remarks

Flow and heat transfer in a turbine cascade with high levels of free-stream turbulence was analyzed using LES with the WALE subgrid-scale model. Results indicate that it is critical to match the experimentally observed state of upstream turbulence approaching the leading edge, as well as to maintain sufficient grid resolution, both upstream of the leading edge and along the vane surface. Ongoing simulations that incorporate these ingredients show improvement in the prediction of transition and heat transfer. Additional sensitivity studies with respect to the impact of turbulence length scale might be needed.

*Acknowledgments*

The authors wish to thank Professor Parviz Moin and the Center for Turbulence Research at Stanford University for their hospitality and technical support. Comments on a draft of this report by Dr. Ivan Bermejo-Moreno are gratefully acknowledged.

REFERENCES

Arts, T., De Rouvroit, M. L. & Rutherford, A. W. 1990 Aero-thermal investigation of a highly-loaded transonic linear turbine guide vane cascade. *Tech. Rep.* 174. Von Karman Institute for Fluid Dynamics.

Bhaskaran, R. & Lele, S. K. 2011 Heat transfer prediction in high-pressure turbine cascade with free-stream turbulence using LES. *AIAA Paper* 2022-3266.

Blair, M. F., Dring, R. P. & Joslyn, H. D. 1989*a* The effects of turbulence and stator/rotor interactions on turbine heat transfer: part I – design operating conditions. *J. Turbomachinery* **111**, 87–96.

Blair, M. F., Dring, R. P. & Joslyn, H. D. 1989*b* The effects of turbulence and stator/rotor interactions on turbine heat transfer: part II – effects of Reynolds number and incidence. *J. Turbomachinery* **111**, 97–103.

Collado Morata, E., Gourdain, N., Duchaine, F. & Gicquel, L. Y. M. 2012 Effects of free-stream turbulence on high pressure turbine blade heat transfer predicted by structured and unstructured LES. *Int. J. Heat Mass Transfer* (on-line).

Joo, J. 2008 Eddy simulation of turbine blade trailing edge cooling. PhD thesis, Stanford University.

Klein, M., Sadiki, A. & Janicka, J. 2003 A digital filter based generation of inflow data for spatially developing direct numerical or large eddy simulations. *J. Comp. Physics* **186**, 652–665.

Lele, S. K. 1992 Compact finite difference schemes with spectral-like resolution. *J. Comp. Physics* **103**, 16–43.

Medic, G. & Sharma, O. P. 2012 Large-eddy simulation of flow in a low-pressure turbine cascade. *ASME Paper* GT2012-68878.

Morgan, B., Larsson, J., Kawai, S. & Lele, S. K. 2011 Improving the low-frequency characteristics of recycling/rescaling inflow turbulence generation. *AIAA Journal* **49** (3), 582–597.

Ni, R. H. 1982 A multiple-grid scheme for solving the Euler equations. *AIAA Journal* **20** (11), 1565–1571.

Nicoud, F. & Ducros, F. 1999 Subgrid-scale stress modeling based on the square of the velocity gradient tensor. *Flow, Turbulence and Combustion* **62**, 183–200.

Sayadi, T., Hamman, C. W. & Moin, P. 2011 Direct numerical simulation of H-type and K-type transition to turbulence. *Center for Turbulence Research Annual Research Briefs* pp. 109–121.

Sayadi, T. & Moin, P. 2011 Predicting natural transition using large-eddy simulation. *Center for Turbulence Research Annual Research Briefs* pp. 97–108.

Wu, X. & Moin, P. 2009 Direct numerical simulation of turbulence in a nominally zero-pressure-gradient flat-plate boundary layer. *J. Fluid Mech.* **630**, 5–41.

Wu, X. & Moin, P. 2010 Transitional and turbulent boundary layer with heat transfer. *Physics of Fluids* **22**, 85–105.

Xiong, Z. & Lele, S. K. 2007 Stagnation-point flow under free-stream turbulence. *J. Fluid Mech.* **590**, 1–33.